An exciton coupled electron transfer process controlled by non-Markovian environments

Souichi Sakamoto* and Yoshitaka Tanimura*

Department of Chemistry, Graduate School of Science, Kyoto University. Sakyoku, Kyoto 606-8502, Japan

E-mail: sakamoto@kuchem.kyoto-u.ac.jp; tanimura@kuchem.kyoto-u.ac.jp

Abstract

We theoretically investigate a conversion process from an exciton transfer (XT) to electron transfer (ET) through an exciton-coupled electron-transfer (XCET) in environments (baths). This XT-ET conversion is essential in a biological and photovoltaic materials for utilization of solar-energy. We develop a handy theoretical model to study the efficiency of XT-ET conversion that occurs either consecutively or concertedly under the influence of non-Markovian baths. A role of quantum coherence between the XT-ET system and the baths is investigated using reduced hierarchal equations of motion (HEOM) that includes three independent baths for the XT, XCET, and ET processes. We found that, while quantum system-bath coherence is important in the XT and ET processes, the coherence among the XT and ET processes has to be suppressed to have an irreversible XT-ET conversion efficiently. This indicates that the XT-ET conversion may be designed to occur consecutively by the virtue of the XCET bath.

Graphical TOC Entry

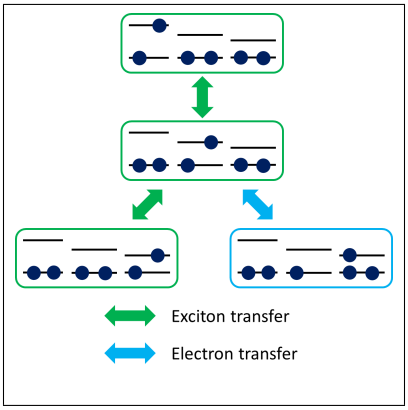

The energy conversion from an exciton transfer (XT) to electron transfer (ET), a XT-ET conversion, plays an essential role in many of biological photosystems and functional molecular materials as the basic mechanism for utilizing solar-energy. Examples involve a photosynthesis[1–13] and solar battery systems.[14–17] In a photosynthesis system including LH1-reaction center and photosystem II, sunlight is absorbed by light-harvesting antenna systems consisting of protein complexes containing light-harvesting ("pigment") molecules, most importantly, chlorophyll. The excitation energy is then transferred through a series of chlorophyll molecules (the XT process) to a reaction center.[1–6] Here, this energy excites a special chlorophyll molecule, which, instead of merely passing on this excitation energy, undergoes charge separation.[10–13] The resulting free electron passes from the chlorophyll molecule to a pheophytin molecule and then to a quinone molecule (The ET process).[7–9]

While these XT and ET processes themselves have been studied extensively, the fundamental mechanism of the irreversible conversion from XT to ET, an XT coupled ET (XCET) process has not yet been established. This conversion mechanism is essential not only as a fundamental problem of chemistry or biochemistry but also for applications such as organic photovoltaic materials.

In this letter, we present a model that describes the XT, ET, and XCET processes. By using this XT-ET model, we can investigate XT-ET conversion dynamics in non-Markovian environments (bath). Special attention will be paid for a role of baths, because the irreversibility in XCET processes arises from the baths. We numerically solved the time evolution of the reduced density matrix elements by employing the hierarchy equations of motion (HEOM) to handle the effect generated from system-bath interaction in a proper way.[18–27]

Although a framework of the present model can be applied varieties of system involving a photovoltaic materials, here we consider a system with N chlorophyll sites as a handy model to investigate the fundamental features of photosynthesis system. Each of chlorophyll sites

are characterized by the HOMO and LUMO levels, as illustrated in TOC. The XT and ET states of the jth site are represented by $|e_j\rangle$ and $|c_j\rangle$, respectively. The states from $j = 1$ to $j = n_{XT}$ are regarded as the XT states, while the states from $j = n_{XT}$ to N states are regarded as the ET states. As illustrated in Fig. 1, the site $j = n_{XT}$ involves both the XT and ET states (XCET states). Thus the conversion from the excited states of pigments in antenna complex to those of reaction center is realized by the sites $j = n_{XT}-1$ and $j = n_{XT}$. The Hamiltonian of the system is[27]

$$\begin{aligned}\hat{\mathcal{H}}_S = &\sum_{i=1}^{n_{XT}} \varepsilon_{\rm i}^{(\rm XT)} |e_i\rangle\langle e_i| + \sum_{i=1}^{n_{XT}-1} (J_{i,i+1}|e_i\rangle\langle e_{i+1}| + h.c.) \\ &+ t_e(|e_{n_{XT-1}}\rangle\langle c_{n_{XT}}| + h.c.) \\ &+ \sum_{j=n_{XT}}^{N} \varepsilon_{\rm j}^{(\rm ET)} |c_j\rangle\langle c_j| + \sum_{j=n_{XT}}^{N-1} t_e(|c_j\rangle\langle c_{j+1}| + h.c.),\end{aligned} \tag{1}$$

where $\varepsilon_{\rm i}^{(\rm XT)}$ and $\varepsilon_{\rm j}^{(\rm ET)}$ are the site energies for the XT states $|e_i\rangle$ and the ET states $|c_j\rangle$, J_{ij} is the XT coupling between $|e_i\rangle$ and $|e_j\rangle$, and t_e is the ET coupling.

The total Hamiltonian is then expressed as

$$\begin{aligned}\hat{\mathcal{H}} &= \hat{\mathcal{H}}_{\mathcal{S}} - \sum_k \hat{V}_k \sum_{\alpha_k} g_{\alpha_k} \hat{x}_{\alpha_k} \\ &+ \sum_k \sum_{\alpha_k} \left(\frac{\hat{p}_{\alpha_k}^2}{2m_{\alpha_k}} + \frac{1}{2} m_{\alpha_k} \omega_{\alpha_k}^2 \hat{x}_{\alpha_k}^2 \right),\end{aligned} \tag{2}$$

where $\hat{V}_k$ is the system part of the coupling and $\hat{x}_{\alpha_k}$, $\hat{p}_{\alpha_k}$, m_{α_k}, and ω_{α_k} are the coordinate, momentum, mass, and frequency of the α_kth oscillator for the kth bath, respectively.

Using this model, we investigated the efficiency of the XT-ET conversion by changing the number of heat-bath and the bath parameters. Then we found that the efficiency of the three-bath model is better than two-bath model, due to the suppression of the quantum coherence between XT and ET processes. Here we present the some of representative results to illustrate this point.

We assume that the XT and XCET states are coupled to the overdamped Drude baths (the XT and XCET baths) described by the spectral distribution, $J_k(\omega) = 2\hbar\lambda_k\gamma_k\omega/\pi(\omega^2 + \gamma_k^2)$ for $k = 1$ and 2,[18–22] while the ET states are coupled to the Brownian mode bath (the ET bath) described by $J_k(\omega) = 2\hbar\lambda_k\gamma_k\omega_0^2\omega/\pi((\omega_0^2 - \omega^2)^2 + \gamma_k^2\omega^2)$ for the index $k = 3$.[23–27] Here, the system bath coupling of XT and ET states are assumed in a diagonal form and are represented by $\hat{V}_1 \equiv \frac{1}{2}(|e_1\rangle\langle e_1| - |e_3\rangle\langle e_3|)$ and $\hat{V}_3 \equiv \frac{1}{2}(|e_4\rangle\langle e_4| - |c_6\rangle\langle c_6|)$, while we consider two kinds of the XCET bath coupling, the off-diagonal (transverse relaxation) form and the diagonal (longitudinal relaxation) form, expressed as $\hat{V}_2^{TR} \equiv (|e_{n_{XT}-2}\rangle\langle e_{n_{XT}-1}| + h.c.)$ and $\hat{V}_2^{LR} \equiv \frac{1}{2}(|e_{n_{XT}-2}\rangle\langle e_{n_{XT}-2}| - |e_{n_{XT}-1}\rangle\langle e_{n_{XT}-1}|)$.

In the photosynthesis case, the XT bath is regarded as the collective modes of antenna system that coupled to the XT states, whereas the ET bath is regarded as the collective modes of reaction center coupled to the ET states. While the bath coupling strength for XT and ET are not weak, that for XCET, which is regarded as the collective modes between the chlorophyll of antenna and that of reaction center, is assumed to be weak, because the distance between the XT and ET systems is assumed to be large. In the same reason we chose J_{34} to be small. The off-diagonal XCET bath coupling may arise from the stretching mode between the XT and ET bride sites.

While the photosynthesis antenna system consists of more than ten XT states, here we set $n_{XT} = 5$ due to the limitation of the CPU power. (See Fig. 1). In order to analyze a role of the baths upon the efficiency of XT-ET conversion process, we study a time evolution of the reduced density matrix from the HEOM approach.[23–27] In this approach, we can investigate system-bath interactions in a non-perturbative and non-Markovian conditions. The bath is characterized by the noise correlation function, $C_k(t) \equiv \langle \hat{X}_k(t)\hat{X}_k(0)\rangle_{\rm B}$, where $\hat{X}_k \equiv \sum_j g_{\alpha_k} x_{\alpha_k}$ is the collective bath coordinate of the kth bath and $\langle \ldots \rangle_{\rm B}$ represents the average taken with respect to the canonical density operator of the baths. When the noise correlation function, $C_k(t)$, is written as a linear combination of exponential functions and a delta function, $C_k(t) = \sum_{j_k=0}^{J_k}(c'_{j_k} + ic''_{j_k})e^{-\gamma_{j_k}|t|} + 2\Delta_k\delta(t)$, which is realized for the

Drude,[18–22] and Brownian[23–27] cases, we can derive the HEOM that consist of the following set of equations of motion for the auxiliary density operators (ADOs) as

$$\begin{aligned}\frac{\partial}{\partial t}\hat{\rho}_{\mathbf{n}_1,\mathbf{n}_2,\mathbf{n}_3}(t) = &-\left[\frac{i}{\hbar}\mathcal{L}+\sum_{k=1}^{3}\sum_{j_k=0}^{J_k} n_{j_k}\gamma_{j_k}\right]\hat{\rho}_{\mathbf{n}_1,\mathbf{n}_2,\mathbf{n}_3}(t)\\ &-\sum_{k=1}^{3}\Delta_k\hat{\Phi}_k^2\hat{\rho}_{\mathbf{n}_1,\mathbf{n}_2,\mathbf{n}_3}(t)\\ &-\sum_{k=1}^{3}\hat{\Phi}_k\sum_{j_k=0}^{J_k}\hat{\rho}_{\ldots,\mathbf{n}_k+\mathbf{e}_{j_k},\ldots}(t)\\ &-\sum_{k=1}^{3}\sum_{j_k=0}^{J_k} n_{j_k}\hat{\Theta}_{j_k}\hat{\rho}_{\ldots,\mathbf{n}_k-\mathbf{e}_{j_k},\ldots}(t),\end{aligned} \tag{3}$$

where $\mathbf{e}_{j_k}$ is the unit vector along the j_kth direction. Here, we defined $\hat{\Phi}_k\hat{\rho} = (i/\hbar)[\hat{V}_k,\hat{\rho}]$, $\hat{\Theta}_{j_k} \equiv c'_{j_k}\hat{\Phi}_k - c''_{j_k}\hat{\Psi}_k$ and $\mathcal{L}\hat{\rho} = [\hat{H}_{\rm S},\hat{\rho}]$. Each ADO is specified by the index $\mathbf{n}_k = (n_{k_{0_k}},\ldots,n_{k_{J_k}})$ with $k = 1$, 2, and 3, where each element takes an integer value larger than zero. The ADO for which all elements are zero, $\mathbf{n}_1 = \mathbf{n}_2 = \mathbf{n}_3 = 0$, corresponds to the actual reduced density operator.

We set the initial populations as $\langle e_1|\hat{\rho}_{\mathbf{0},\mathbf{0},\mathbf{0}}|e_1\rangle = 1.0$ and other diagonal elements of the reduced density matrix as 0. Experimentally, this condition is created by a short laser pulse. We fix the characteristic frequency of third bath as $\omega_0 = 500\text{cm}^{-1}$ and use it as the unit of the system.

The site energies of XT and ET states are chosen to be $\varepsilon_1^{(\text{XT})} = \varepsilon_3^{(\text{XT})} = 0.6\omega_0$, $\varepsilon_2^{(\text{XT})} = \varepsilon_5^{(\text{XT})} = 0.2\omega_0$, $\varepsilon_4^{(\text{XT})} = 0.0$, $\varepsilon_5^{(\text{ET})} = \omega_0$ and $\varepsilon_6^{(\text{ET})} = 0.0$. We construct an energy scheme of the model by adapting the funnel concept, in which, as XT proceeds, site energy of each state decreases, as observed in Photosystem II.[28]

Throughout this letter, we fix the inverse temperature $\beta\hbar\omega_0 = 2.4(300\text{ K})$. For system coupling parameters, we set $J_{12} = J_{23} = 0.6\omega_0$, $J_{34} = 0.02\omega_0$, $J_{45} = 0.1\omega_0$, and $t_e = 0.2\omega_0$ for a photosynthesis system in mind. We chose the XCET system coupling, J_{34}, is relatively small in comparison with J_{12} and J_{45}, reflecting the fact that the distance between the

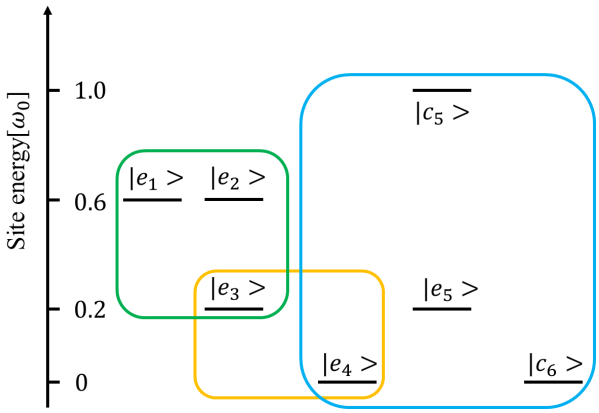

Figure 1: Schematic view of a model system. The model system described by the Hamiltonian Eqs.(1) and (2). Here, $|e_i\rangle$ and $|c_j\rangle$ represent the XT and ET states at the site j. The green, blue, and orange square represent the XT bath of antenna system, the ET bath of the reaction center, and the XCET bath for XT and ET bridge states, respectively.

chlorophylls in antenna and reaction center systems is large. We set other $J_{ij} = 0.0$. The bath coupling strengths (reorganization energy) are chosen to be $\lambda_1 = 0.5\omega_0$, $\lambda_3 = 0.1\omega_0$, and $\gamma_k = 0.1\omega_0$ for $k = 1$, 2, and 3. The HEOM given by Eq. (3) were then numerically integrated via the fourth-order Runge-Kutta method, in which the time step is 0.01 / ω_0. We chose the depth of the hierarchy and the truncation number of the hierarchy $\mathrm{N_{max}} = 8$.

Figure 2 illustrates the time evolution of density matrix elements for (a) a weak and (b) strong diagonal-XCET bath coupling cases. In the weak coupling case in Fig. 2(a), the population states of antenna system exhibit coherent oscillations, but the populations do not transfer to the ET population states. This is because pure dephasing becomes a dominant effect of the XCET bath in this diagonal coupling case, while the population relaxation becomes a dominant effect in the off-diagonal coupling case.[29] Because pure dephasing merely fluctuate the exciton energy sites and does not contribute to the transporting energy, the XT from $|e_3\rangle$ to $|e_4\rangle$ is small. Thus the population of $|c_6\rangle$ does not increase. For the strong diagonal coupling case in Fig. 2 (b), the population of $|e_4\rangle$ slowly increases through the J_{34} interaction due to the relaxation arises from the strong diagonal XCET bath coupling. Even under this strong coupling case, however, the efficiency of the transition from XT to ET is considerably smaller than the off-diagonal case as we explain below.

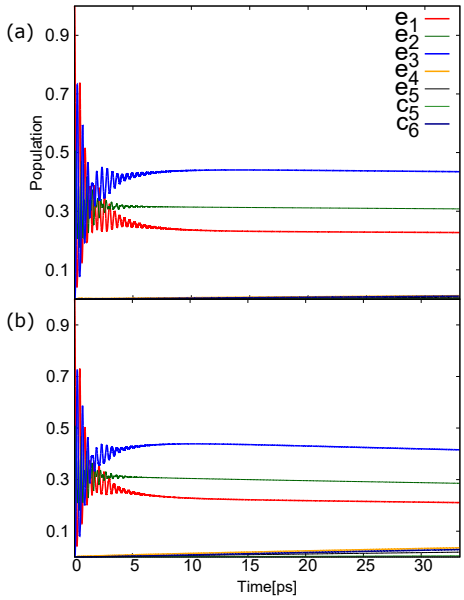

Figure 2: Time evolution of the density matrix for (a) the weak ($\lambda_2 = 0.01\omega_0$) and (b) strong ($\lambda_2 = 0.1\omega_0$) diagonal XCET bath coupling ($\hat{V}_2^{LR}$) cases, The XCET transition strength is chosen to be weak, $J_{34} = 0.02\omega_0$. In each figure, dashed and solid curves represent the population of the XT and ET states, respectively.

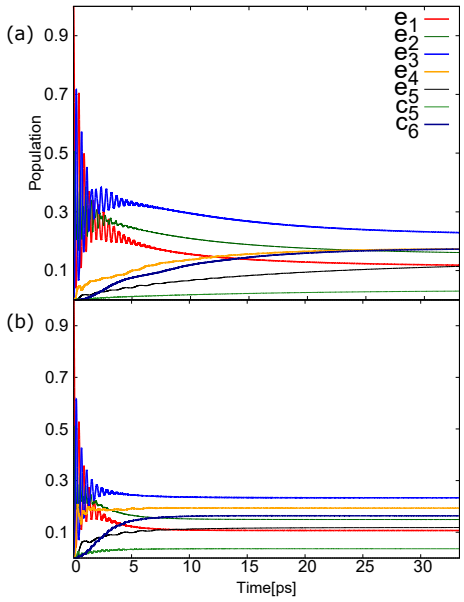

Figure 3: Time evolution of the density matrix for (a) the weak ($\lambda_2 = 0.01\omega_0$) and (b) strong ($\lambda_2 = 0.1\omega_0$) off-diagonal XCET bath coupling ($\hat{V}_2^{TR}$) cases. In each figure, dashed and solid curves represent the population of the XT and ET states, respectively.

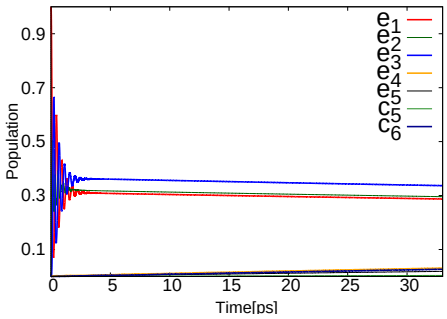

Figure 4: Time evolution of the density matrix for two-bath case. Here, the second bath is incorporated into the first Drude bath. For this incorporated bath, we set $\hat{V}_1' = \hat{V}_1 + \alpha_2 \hat{V}_2^{TR}$ with $\alpha_2 = 0.01$. The other parameters are the same as in the case in Fig. 3(a).

Figure 3 illustrates the time evolution of density matrix elements for off-diagonal-XCET bath coupling. In both (a) the weak and (b) strong coupling cases, the efficiency of transition is much larger than the diagonal modulation case depicted in Fig. 2. While the $|c_6\rangle$ population increases monotonically following the increase of the $|e_4\rangle$ population in the weak case, those in the strong case reach the quasi-steady state quickly. After the $|e_4\rangle$ site is populated, the coherent ET transition occurs from the $|e_4\rangle$ site to the $|e_6\rangle$ site via $|c_5\rangle$ site by a super-exchange mechanism,[7] in which the ET bath with Brownian mode plays an essential role.[24–26] Although here we included the $|e_5\rangle$ site, it does not play any major role, because the transition from the $|e_5\rangle$ to $|c_6\rangle$ sites is prohibited. When the population reaches the $|c_6\rangle$ state, it does not return to the $|e_4\rangle$ site, because the distribution is close to the equilibrium states through super-exchange mechanism. These results of calculation indicate that the bath effectively enhances the transition even under weak exciton coupling regime ($J_{34} = 0.02$), in particular the transition between antenna complexes and reaction center in photosynthesis.

While the strong XCET bath coupling may not be realistic for the photosynthesis system, the mechanism utilizing off-diagonal weak coupling bath is conceivable to achieve efficient XT-ET transition. Moreover, the final population in the strong coupling case is smaller than the that in the weak coupling case, because the off-diagonal coupling acts as the damper for the XCET transition in the strong coupling case, while it acts as the thermal activator

in the weak coupling case. Equilibration time for the weak coupling case is approximately 30ps, which agrees with the experimentally estimated time scale between the antenna and reaction center in a photosynthesis system.

It should be noted that if we consider a single bath from the $|e_1\rangle$ to $|e_4\rangle$ sites, by incorporating the second XCET bath into the first XT bath, the final population does not increase efficiently due to the coherence between the $|e_3\rangle$ and $|e_4\rangle$ states. To illustrate this point, we present the calculated results for this XT and ET baths case in Fig.4. Here, the system-bath correlations in the XT process and the ET process overlap via the $|e_4\rangle$ state. The increase of population in the XT and ET baths case is notably smaller than that in the three baths case, while $\hat{V}_2^{LR}$ is chosen to be the same as in the case in Fig. 3(a).

This result indicates that, to have an efficient XT-ET conversion, the coherence in the XT process should be suppressed in the bridge state, $|e_4\rangle$, because otherwise the population in the $|e_4\rangle$ does not increase due to the collective coherent motion in the XT states. The XCET bath plays a key role to suppress the coherence in the XT sites. This implies that the XT-ET conversion occurs consecutively rather than concertedly due to the interaction with the XCET bath. This mechanism indeed enhances the conversion rate.

For further investigation, we must extend the present model for larger system and more realistic parameter.[10–12] We leave it for a future study.

Acknowledgments

This research is supported by a Grant-in-Aid for Scientific Research (A26248005) from the Japan Society for the Promotion of Science.

References

(1) A. Ishizaki and G. R. Fleming, Proc. Natl. Acad. Sci. USA, **106**, 17255 (2009).

(2) Y. Fujihashi, G. R. Fleming, and A. Ishizaki, **142**, 212403 (2015).

(3) J. Struempfer and K. Schulten, J. Chem. Phys. **131**, 225101 (2009).

(4) J. Struempfer and K. Schulten, J. Chem. Phys. **134**, 095102 (2011).

(5) J. Struempfer and K. Schulten, J. Chem .Phys. **137**, 065101 (2012).

(6) C. Kreisbeck and T. Kramer, J. Phys. Chem. Lett. **3**, 2828 (2012).

(7) H. Sumi and T. Kakitani, Phys. Chem. Phys. Lett., **252**, 85 (1996).

(8) V. I. Novoderezhkin, E. Romero, J. P. Dekker, and R. van. Grondelle, Phys. Chem. Phys. Chem, **12**, 681 (2011).

(9) V. I. Novoderezhkin, E. Romero, and R. van. Grondelle, Phys. Chem. Chem. Phys. **17**, 30828 (2015).

(10) K. E. Dorfman, D. V. Voronine, S. Mukamel, and M. O. Scully, Proc. Natl. Acad. Sci. USA, **110**,2746 (2012).

(11) F. Muh, M. Plockinger, H. Ortmayer, M. Schmidt am Busch, D. Lindorfer, J. Adolphs, T. Renger J. Photochem. Photobiol. B. **152**, 286 (2015).

(12) M. K. Lee, D. Coker, **xxxx**, xxxx (2017).

(13) T. Kramer, M. Rodriguez, and Y. Zelinskyy, J. Phys. Chem. B, **121**, 463 (2017).

(14) Gelinas, S. Rao, A. Kumar, A. Smith, S. L. Chin, A. W. Clark, and J. van .der. Poll, T. S. Science, **343**, 512 (2014).

(15) J. Zirzlmeier, D. Lehnherr, P. B. Coto, E. T. Chernick, R. Casillas, B. S. Basel, M. Thoss, R. R. Tykwinski, and D. M. Guldi, Proc. Natl. Acad. Sci. USA, **112**, 5325 (2015).

(16) H. Tamura and I. Burghardt, J. Am. Chem. Soc. **135**, 16364 (2013).

(17) M. Huix-Rotllant, H. Tamura, I. Burghardt. J. Phys. Chem. **6**, 1702 (2015).

(18) Y. Tanimura and R. Kubo, J. Phys. Soc. Jpn. **58**, 101 (1988).

(19) A. Ishizaki and Y. Tanimura, J. Phys. Soc. Jpn. **74**, 3131 (2005).

(20) Y. Tanimura, J. Phys. Soc. Jap. **75**, 082001 (2006).

(21) Y. Tanimura, J. Chem. Phys. **141**, 044114 (2014).

(22) Y. Tanimura, J. Chem. Phys. **142**, 144110 (2015).

(23) Y. Tanimura and S. Mukamel, J. Phys. Soc. Jpn. **63**, 66 (1994).

(24) M. Tanaka and Y. Tanimura, J. Phys. Soc. Jpn. **78**, 073802 (2009).

(25) M. Tanaka and Y. Tanimura, J. Chem. Phys. **132**, 214502 (2010).

(26) Y. Tanimura, J. Chem. Phys. **137**, 22A550 (2012).

(27) A. G. Dijkstra and Y. Tanimura, J. Chem. Phys. **142**, 212423 (2015).

(28) Robert E. Blankenship, (2014) Molecular Mechanisms of Photosynthesis, 2nd Ed. Wiley-Blackwell, Oxford, UK.

(29) A. Ishizaki and Y. Tanimura, J. Chem. Phys. **125**, 084501 (2006).